



Original paper

## Quantitative evaluation of image recognition performance of fiducial markers in real-time tumor-tracking radiation therapy



Naoki Miyamoto<sup>a,b,\*</sup>, Kenichiro Maeda<sup>c</sup>, Daisuke Abo<sup>d</sup>, Ryo Morita<sup>d</sup>, Seishin Takao<sup>e</sup>,  
Taeko Matsuura<sup>a,b</sup>, Norio Katoh<sup>b,f</sup>, Kikuo Umegaki<sup>a,b</sup>, Shinichi Shimizu<sup>b,g</sup>, Hiroki Shirato<sup>b,f</sup>

<sup>a</sup> Division of Quantum Science and Engineering, Faculty of Engineering, Hokkaido University, North 13, West 8, Kita-ku, Sapporo, Hokkaido 060-8638, Japan

<sup>b</sup> Global Station for Quantum Medical Science and Engineering, Global Institution for Collaborative Research and Education (GI-CoRE), Hokkaido University, North 14, West 5, Kita-ku, Sapporo, Hokkaido 060-8648, Japan

<sup>c</sup> Hokkaido University Hospital Clinical Research and Medical Innovation Center, Hokkaido University, North 14, West 5, Kita-ku, Sapporo, Hokkaido 060-8648, Japan

<sup>d</sup> Department of Diagnostic and Interventional Radiology, Hokkaido University Hospital, North14, West 5, Kita-ku, Sapporo, Hokkaido 060-8638, Japan

<sup>e</sup> Proton Beam Therapy Center, Hokkaido University Hospital, North14, West 5, Kita-ku, Sapporo, Hokkaido 060-8638, Japan

<sup>f</sup> Department of Radiation Medicine, Faculty of Medicine, Hokkaido University, North 15, West 7, Kita-ku, Sapporo, Hokkaido 060-8638, Japan

<sup>g</sup> Department of Radiation Medical Science and Engineering, Faculty of Medicine, Hokkaido University, North 15, West 7, Kita-ku, Sapporo, Hokkaido 060-8638, Japan

### ARTICLE INFO

#### Keywords:

Fiducial marker  
Image recognition  
Real-time tumor-tracking radiation therapy  
Image-guided radiation therapy

### ABSTRACT

**Purpose:** To quantitatively evaluate and compare the image recognition performance of multiple fiducial markers available in real-time tumor-tracking radiation therapy (RTRT).

**Methods:** Clinically available markers including sphere shape, coil shape, cylinder shape, line shape, and ball shape (folded line shape) were evaluated in liver and lung models of RTRT. Maximum thickness of the polymethyl methacrylate (PMMA) phantom that could automatically recognize the marker was determined by template-pattern matching. Image registration accuracy of the fiducial marker was determined using liver RTRT model. Lung RTRT was mimicked with an anthropomorphic chest phantom and a one-dimensional motion stage in order to simulate marker motion in heterogeneous fluoroscopic images. The success or failure of marker tracking and image registration accuracy for the lung model were evaluated in the same manner as that for the liver model.

**Results:** All fiducial markers except for line shape and coil shape of thinner diameter were recognized by the PMMA phantom, which is assumed to have the typical thickness of an abdomen, with two-dimensional image registration accuracy of < 2 pixels. Three-dimensional calculation error with the use of real-time stereoscopic fluoroscopy in RTRT was thought to be within 1 mm. In the evaluation using the lung model, the fiducial markers were recognized stably with sufficient accuracy for clinical application. The same was true for the evaluation using the liver model.

**Conclusions:** The image recognition performance of fiducial markers was quantified and compared. The results presented here may be useful for the selection of fiducial markers.

### 1. Introduction

Fiducial markers are utilized for accurate patient setup as well as for evaluating the range of inter- and intrafractional organ motion in the context of image-guided radiation therapy [1–4]. Visibility of the fiducial markers that are used in clinical practice has been evaluated based on visual inspection in the settings of kilovoltage imaging, megavoltage imaging, computer tomography, and magnetic resonance imaging [5–9]. Treatments that utilize automatic marker recognition technique in combination with fiducial markers in sequential images during radiation therapy [e.g., real-time tumor-tracking radiation

therapy (RTRT) [10,11]] require quantitative evaluations of the image recognition performance of fiducial markers. The RTRT system consists of a linear accelerator and two X-ray fluoroscopy devices. The three-dimensional position of the inserted fiducial marker is calculated from the projected position in the pair of fluoroscopic images obtained in two different directions. Image-processing techniques such as template-pattern matching are used to locate the projected position of the fiducial marker for automatic image registration [12–14]. Treatment beam irradiation is enabled only when the calculated three-dimensional position of the fiducial marker is within a pre-defined region called the gating window. In this way, gated beam irradiation can be administered

\* Corresponding author at: Faculty of Engineering, Hokkaido University, North 13, West 8, Kita-ku, Sapporo, Hokkaido 060-8638, Japan.

<https://doi.org/10.1016/j.ejmp.2019.08.004>

Received 17 March 2019; Received in revised form 1 August 2019; Accepted 2 August 2019

Available online 12 August 2019

1120-1797/ © 2019 Associazione Italiana di Fisica Medica. Published by Elsevier Ltd. All rights reserved.

to mobile targets in the lung or liver.

Image quality of the X-ray images obtained with RTRT is different from that of images acquired using on-board imaging (OBI). For instance, typical settings for kV image acquisition in OBI for chest and abdomen are 10 mAs and 32 mAs, respectively [15], whereas the RTRT system makes use of pulsed fluoroscopy with up to about 0.5 mAs, with relatively large source-to-image distance (SID) of approximately 4 m. RTRT requires performance checks with sequential images obtained by pulsed fluoroscopy in a model clinical situation because image quality and search images of fiducial markers vary from image to image, according to respiratory motion. To date, few reports have quantitatively evaluated the image recognition performance of multiple fiducial markers that can be used for RTRT.

The purpose of this study is to quantify the image recognition performance of fiducial markers and to provide reference information for marker selection. Thus, we evaluated clinically available markers including sphere shape, coil shape, cylinder shape, line shape, and ball shape (folded line shape) using liver and lung RTRT models. Because the projected pattern of marker and image contrast in two-dimensional images may be varied according to imaging angle for non-spherical markers, all evaluations were conducted in three typical imaging directions.

## 2. Materials and methods

### 2.1. Fiducial markers evaluated

The characteristics of the fiducial markers evaluated in this study are summarized in Table 1. Representative fluoroscopic images for each fiducial marker and each imaging angle are shown in Fig. 1.

Image recognition performance was evaluated for all fiducial markers using liver and lung RTRT clinical models. In this study, imaging situation in liver RTRT was mimicked by the polymethyl methacrylate (PMMA) slab phantom. The maximum thickness of the PMMA slab phantom for which the marker can be tracked automatically by means of template-pattern matching was evaluated as one of the indices of recognition performance. The accuracy of two-dimensional image registration of each fiducial marker was also evaluated in fluoroscopic images. Lung RTRT was mimicked using an anthropomorphic chest phantom (Lungman, Kyoto Kagaku, Japan) and a one-dimensional motion stage in order to simulate the marker motion in heterogeneous fluoroscopic images. Actual tumor motion sometimes includes hysteresis. It was assumed that marker recognition performance was not affected by hysteresis in this study since the image quality around the fiducial marker in each image was similar in this experimental setup. Success or failure of the marker tracking and image registration accuracy were evaluated in the same manner as those for the liver model. In order to confirm dependency on the imaging angle, evaluations were conducted with three imaging angles for all markers except for the Gold Marker, iGold, and ball-shaped Gold Anchor. The dependency on the imaging angle was not evaluated for the spherical shape markers since the projection image of such markers is almost circular at any imaging

angle.

### 2.2. Liver model: Maximum recognizable PMMA thickness and registration accuracy

The experimental setup and geometry are shown in Fig. 2. X-ray fluoroscopic imaging was performed with an X-ray tube (UD-150-B40/0.6/1J317C-282, SHIMADZU, Japan) and flat-panel detector (PaxScan 3030, Varian Medical Systems, USA). The fiducial markers were placed at the isocenter, and thickness of the PMMA plate was varied from 10 cm to 30 cm, in increments of 1 cm. Image recognition performance would not be varied significantly when the fiducial marker was inside or outside the PMMA phantom since the effect of scattered radiation which was one of the main components to degrade the visibility of the fiducial marker was expected to be similar for each case in this imaging geometry. For pulsed fluoroscopy, tube voltage and pulse width were fixed at 110 kVp and 4 ms (maximum for the respective experimental device). In order to evaluate the dependency on imaging dose, evaluation was conducted at X-ray tube current values of 50, 80, and 160 mA as low-dose, middle-dose, and high-dose imaging, respectively. Image acquisition was conducted for all combinations for each fiducial marker, PMMA thickness, and imaging dose. One hundred images were acquired for each imaging condition. For each marker, the template image for template-pattern matching was created from the first fluoroscopic image obtained without the PMMA phantom. For the evaluation of image registration accuracy, average position of the recognized marker without using the PMMA phantom was determined as the reference position. In this study, a function of template-pattern matching included in the Matrox Imaging Library (Matrox Electronic Systems Ltd., Canada) was used to locate the position of the marker in fluoroscopic images. Template-pattern matching is based on normalized cross correlation. The correlation coefficient is given by

$$r = \frac{N \sum_{i=1}^N I_i M_i - (\sum_{i=1}^N I_i) (\sum_{i=1}^N M_i)}{\sqrt{|N \sum_{i=1}^N I_i^2 - (\sum_{i=1}^N I_i)^2| |N \sum_{i=1}^N M_i^2 - (\sum_{i=1}^N M_i)^2|}} \quad (1)$$

where  $N$  is the pixel number, and  $I_i$  and  $M_i$  are the pixel values of the target image and the template image, respectively. The location that gives the highest  $r$  is considered to be the marker position in the search area. Image registration accuracy was defined as the root mean square error (RMSE) of the difference between the recognized two-dimensional marker position acquired with template-pattern matching and the reference marker position. Since it was difficult to obtain similar image quality in two orthogonal fluoroscopic images in this experimental setup, three-dimensional error was estimated from two-dimensional RMSE. With considering the imaging geometry of RTRT using triangulation method for three-dimensional calculation [10], three-dimensional positional error can be equivalent to two-dimensional image registration error. Template-pattern matching was conducted image by image. Image recognition was considered successful when the difference between the recognized marker position and the reference marker position was less than the size of the fiducial marker. In cases where the rate of successful image recognition was > 95% in the evaluation of 100 frames, the fiducial marker was considered to have sufficient accuracy at for tracking at the PMMA thickness examined. In this study, if a marker could be tracked with a PMMA of thickness  $\geq 22$  cm (typical abdomen thickness) [16], at any imaging dose, the marker was considered to be sufficiently accurate for use in liver RTRT. Because projected pattern changed according to imaging angle, evaluations of non-spherical markers including the VISICOIL, ACCULOC, and line-shaped Gold Anchor were conducted with three imaging angles, as shown in Fig. 2. For evaluation of the VISICOIL and line-shaped Gold Anchor with imaging angle of  $90^\circ$  and  $45^\circ$ , the tip of the fiducial marker was tracked. For these line-shaped markers, criteria of successful image recognition were determined to be the largest dimension, which was about 2 mm, of the marker in the template image.

**Table 1**

Fiducial markers evaluated in this study.

Product name, Manufacture	Shape	Dimension
Gold Marker <sup>a</sup> , OLYMPUS	sphere	diameter: 1.5 mm
iGold <sup>a</sup> , MEDIKIT	sphere	diameter: 2.0 mm
VISICOIL, IBA	coil	length: 10 mm, diameter: 0.35, 0.5, 0.75, and 1.1 mm
Gold Anchor, Naslund Medical Inc.	line shape	length: 10, 20 mm
ACCULOC, CIVCO	ball shape	diameter: approximately 2 mm
	cylinder	length: 3 mm, diameter: 0.9, 1.2 and 1.6 mm

<sup>a</sup> Currently distributed only in Japan.

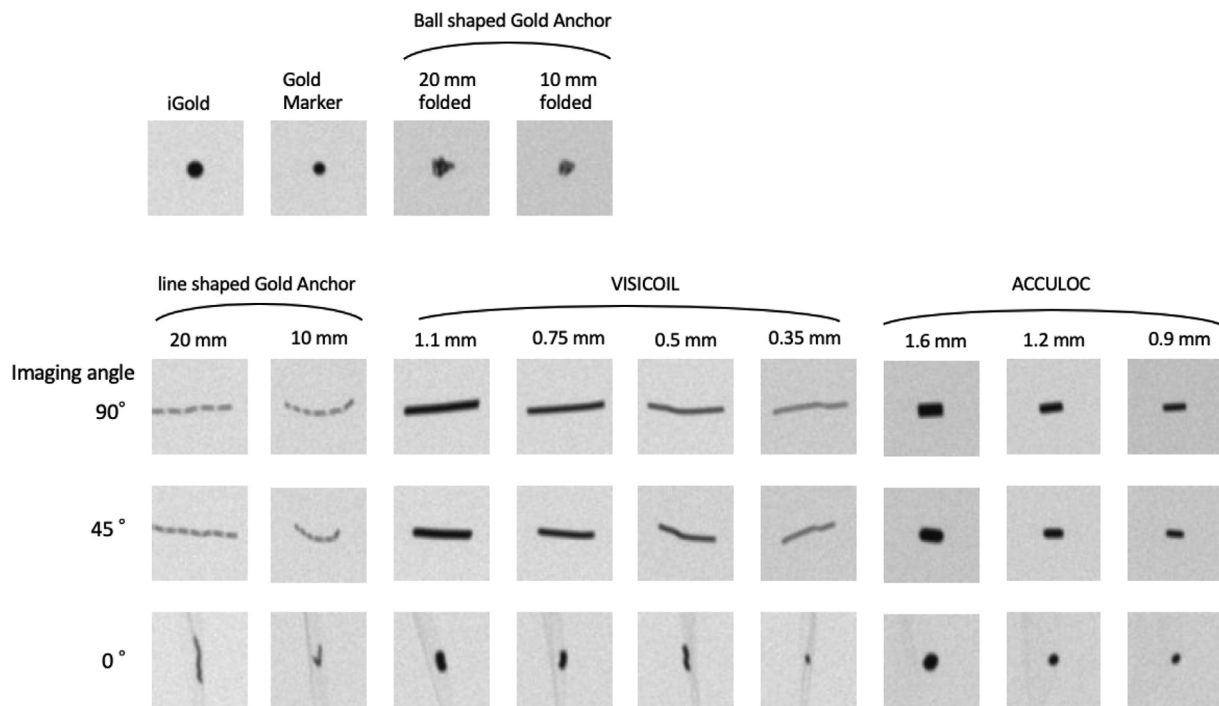


Fig. 1. Representative fluoroscopic images of the fiducial markers acquired with imaging. Window-level settings were the same for all images. For non-spherical markers, imaging angle is provided.

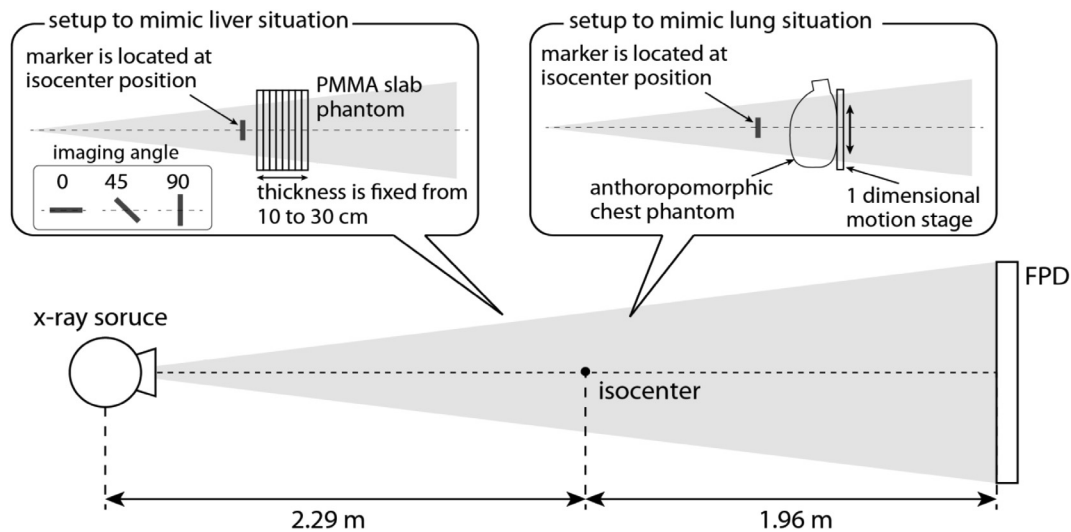


Fig. 2. Experimental setup and imaging geometry.

2.3. Lung model: tracking in heterogeneous images and registration accuracy

Experimental setup and imaging geometry were the same as depicted in Fig. 2. A one-dimensional motion stage and an anthropomorphic chest phantom (Lungman, Kyoto Kagaku, Japan) were used. The fiducial marker was fixed at the isocenter position. By moving the chest phantom with the motion stage, image variation due to respiration was simulated. The motion stage was moved sinusoidally with a cycle of 3 s and amplitude of 20 mm. Image registration error was evaluated by comparing recognized fixed marker position and position of the reference marker, as determined without the chest phantom. For mimicking lung parameters, image recognition performance was evaluated in two scenarios by adjusting the position of the chest phantom. In one scenario, the marker image was projected in the lung region,

overlapping with the ribs, in order to mimic background image contrast with low variation. In the other scenario, the marker image was projected onto the lung region, overlapping with the vertebrae, to simulate substantial variation in background image contrast. For each scenario, marker recognition performance was evaluated with three imaging doses in order to evaluate the dependency on imaging dose. In lung/rib scenario, tube voltage and pulse width were fixed to 80 kVp and 4 ms, respectively. Tube current was set to 25, 50, and 80 mA. In the lung/vertebrae scenario, tube voltage and pulse width were fixed to 100 kVp and 4 ms, respectively; tube current settings were 25, 50, and 80 mA. The success or failure of marker tracking and image registration accuracy were evaluated in the same manner as that described for the liver model.

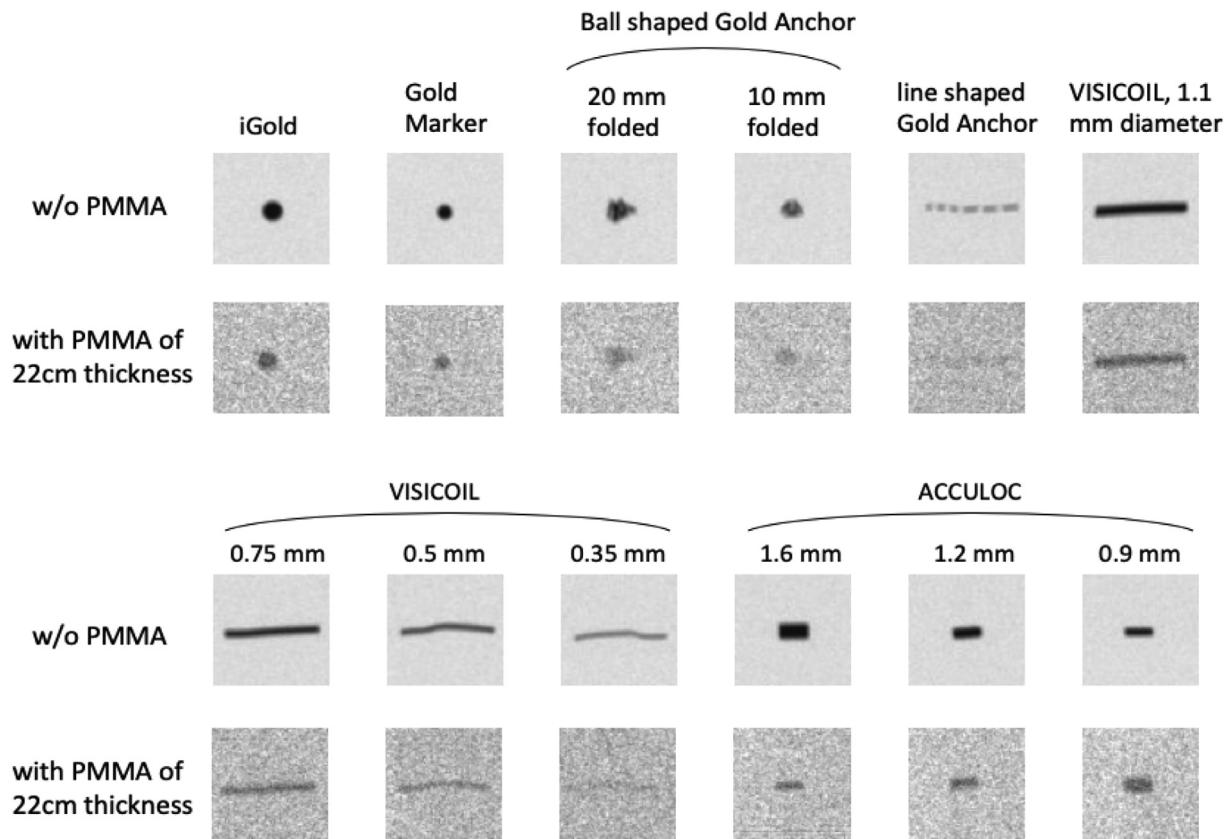


Fig. 3. Representative fluoroscopic images of fiducial markers with or without PMMA phantom.

### 3. Results

#### 3.1. Liver model: maximum recognizable PMMA thickness and registration accuracy

Representative fluoroscopic images of fiducial markers obtained with and without the use of a PMMA phantom (22-cm thickness) are shown in Fig. 3. Compared with other markers, the thinner-diameter VISICOIL and the line-shaped Gold Anchor showed decreasing visibility as PMMA thickness increased. Maximum PMMA thickness for which the fiducial marker could be tracked at each imaging dose is shown in Fig. 4. Because image quality improved by high-dose imaging, the

maximum thickness in high-dose imaging was greater than that in low-dose imaging for all markers. Maximum PMMA thickness for which the fiducial marker could be tracked at each imaging angle is shown in Fig. 4. Less dependency on imaging angle was found for ACCULOC and VISICOIL of  $\geq 0.75$  mm diameter. The data revealed substantial dependency on imaging angle for the line-shaped Gold Anchor and VISICOIL of  $\leq 0.5$  mm diameter. With use of these markers, image contrast sufficient for template-pattern matching could not be obtained for fiducial markers because of small X-ray attenuation at certain imaging angles. For these reasons, the fiducial markers listed above are not recommended for use in RTRT because stable automatic image recognition is difficult.

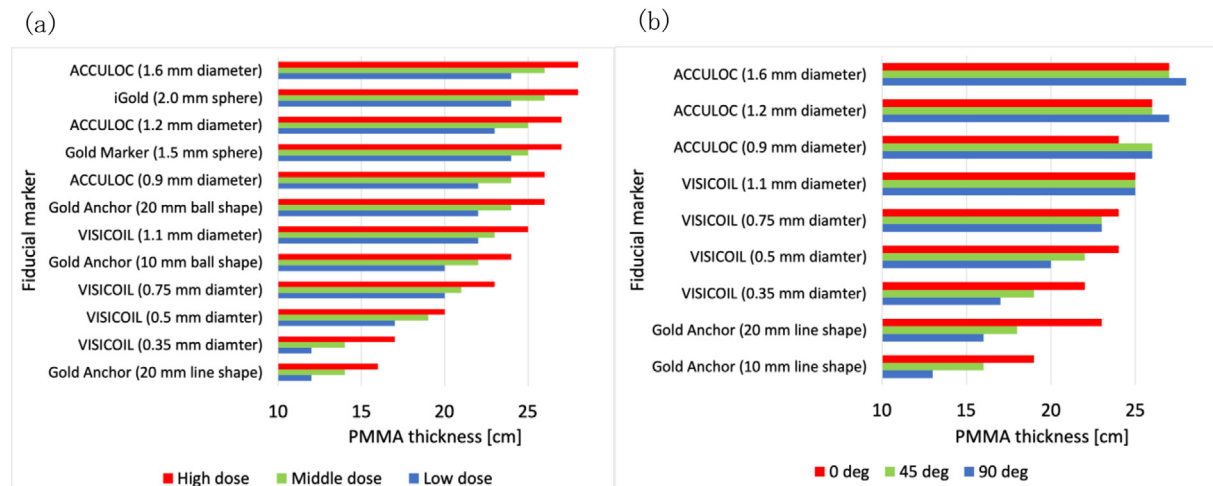


Fig. 4. (a) Maximum PMMA thickness for each fiducial marker in each imaging condition (90° imaging angle). (b) Maximum PMMA thickness for each marker at each imaging angle.

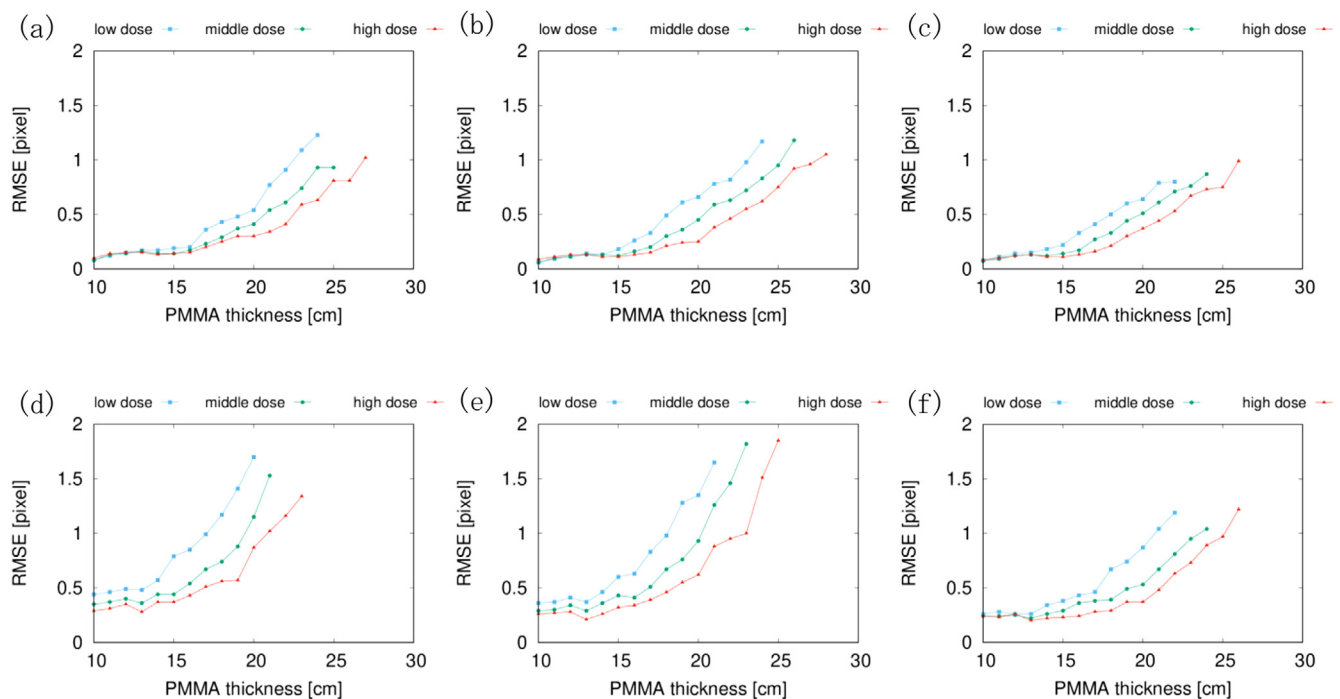


Fig. 5. RMSE of image recognition for each fiducial marker, PMMA thickness, and imaging dose. (a) Gold Marker, (b) iGold, (c) ball-shaped Gold Marker (20-mm length), (d) VISICOIL of 0.75-mm diameter, (e) VISICOIL of 1.1-mm diameter, (f) ACCULOC of 0.9-mm diameter.

The image registration accuracy of fiducial markers at each imaging dose is presented in representative images in Fig. 5. For all markers, image registration accuracy decreased with increasing PMMA thickness because of decreased image quality. RMSE for two-dimensional image registration with successful tracking was  $< 2$  pixels, which corresponded to approximately 0.2 mm. These fiducial markers are expected to track stably in liver models.

In RTRT, the three-dimensional position of a fiducial marker is evaluated from two projected positions, which are determined by template-pattern matching for each image. The calculated three-dimensional position may therefore be over- or underestimated if there is a discrepancy between the three-dimensional representative point and its projected position on the image. In the case of spherical markers, the projected images are always circular, and it is easy to determine the projected centroid position by using a template image that has been prepared in advance. As a result, three-dimensional centroid position can be accurately derived. For non-spherical markers such as VISICOIL, the template image should be created separately for each treatment, with consideration to the correspondence of three-dimensional position and projected position, because the projected image may differ among treatments. Three-dimensional imaging coordinate calculations may also carry calibration error. Assuming the imaging geometry of SyncTraX (SHIMADZU, Japan), which can be combined with general linac to conduct RTRT, the total accuracy of three-dimensional calculation is expected to be within 1 mm. Note that the evaluated performance of fiducial markers may depend on imaging geometry, characteristics of imaging device and X-ray technique (e.g., tube energy, current, pulse width).

### 3.2. Lung model: tracking in heterogeneous images and registration accuracy

Representative heterogeneous fluoroscopic images for fiducial markers under conditions mimicking lung RTRT are shown in Fig. 6. Image recognition by template-pattern matching was difficult with VISICOIL of  $\leq 0.5$  mm diameter and with the line-shaped Gold Anchor, because the distinction between marker and background image was

difficult due to low contrast. These markers could be tracked at limited imaging angles under high-dose imaging conditions. These fiducial markers are not recommended for use in RTRT because stable automatic image recognition is difficult. Other fiducial markers that were successfully recognized in heterogeneous images that varied frame by frame may be used for lung RTRT.

Image registration accuracy for representative fiducial markers, as evaluated in two lung scenarios, is presented in Fig. 7. In cases where the marker image overlapped with lung and vertebrae, as opposed to lung and ribs, image recognition accuracy was slightly decreased due to the high variation in image contrast. In the case of successful tracking, RMSE for two-dimensional image registration was  $< 1$  pixel for all fiducial markers, and three-dimensional calculation error was expected to be within 1 mm.

## 4. Discussion

In RTRT, irradiation is administered only when the calculated three-dimensional position of the fiducial marker is within the allowed region, called the “gating window”. Under typical conditions, the gating window is determined as the cubic region, the center of which corresponds to the representative point of the fiducial marker in CT images obtained preoperatively. The discrepancy between the center of the gating window as the representative point of the fiducial marker which is to be tracked and the actual tracked position will lead to systematic error in the beam irradiation administered. With spherical markers, high consistency can be between the center of the gating window and the tracking position may be achieved because the center of the marker can be easily identified in CT images. With non-spherical markers, the identification of the representative marker point in the CT images could be difficult because the marker shape and metal artifact depend on the marker angle and folding condition. Assuming the worst-case scenario, a few millimeters of systematic error of the beam irradiation may occur if the center of gravity of the marker is defined as the center of the gating window in CT images and the tip of the marker is tracked during treatment. The evaluation of any possible discrepancy should be performed according to the way in which the fiducial marker is used. In

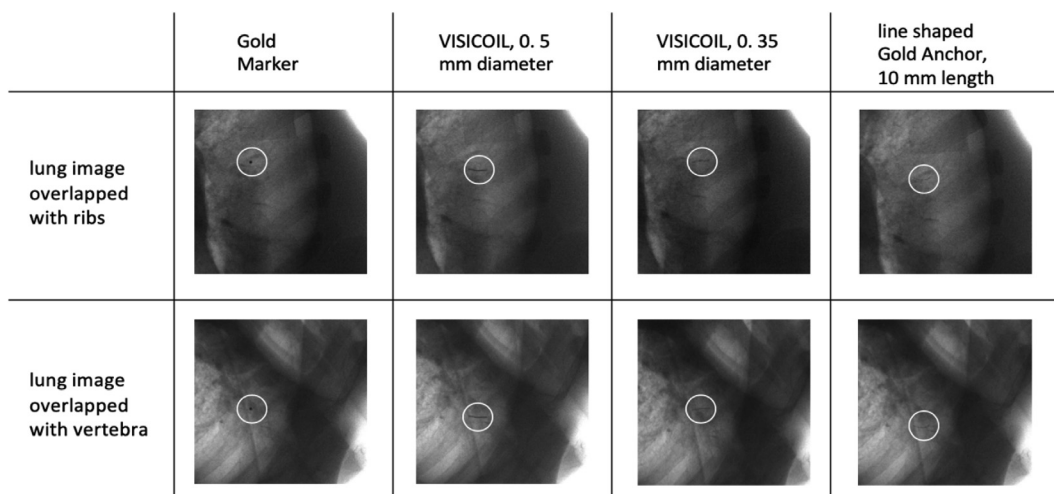


Fig. 6. Representative fluoroscopic images of markers with use of the chest phantom.

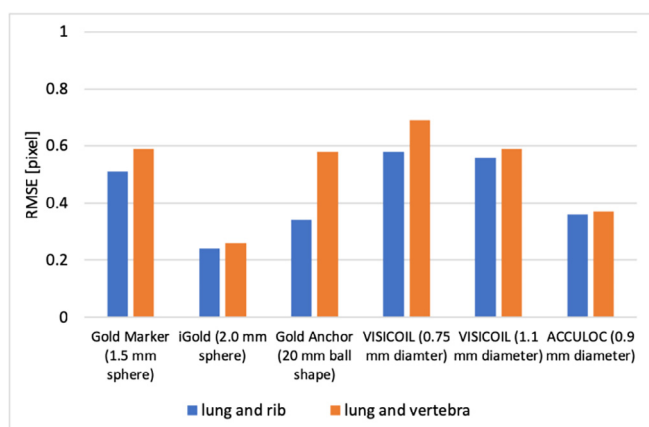


Fig. 7. RMSE of image recognition for each fiducial markers in two lung scenarios (lung/ribs and lung/vertebrae).

clinical use, possible error should be assessed and compensated for with the appropriate margins during treatment planning.

Marker selection should be performed with consideration to the dosimetric distortion caused by internal fiducial markers. Fiducial markers containing large or high-Z material will show high image recognition performance as shown in our results. However, dose perturbation increases with use of these markers [17]. Uncertainty in dose calculation will be increased because the metal artifact in the CT image will become larger. Studies of internal fiducial markers in proton therapy have shown that irradiation from multiple angles can compensate for dosimetric perturbation [18]. Dosimetric perturbation is also observed in photon therapy [19].

In addition to considerations of image recognition performance and dosimetric effect, the marker should be selected after attention is given to the invasiveness of marker insertion and positional stability after insertion. For instance, assuming that invasiveness may be defined as the size of the insertion needle, Gold Anchor might be considered as minimally invasive, because it can be implanted percutaneously using a 25-gauge needle. However, application of the Gold Anchor may be limited to patients of standard or thin physical constitution. The image recognition performance of Gold Anchor will be lower than that of the spherical markers and ACCULOC. There is a possibility that percutaneous insertion may induce pneumothorax [20,21]. There is no risk of pneumothorax in the case of bronchoscopic insertion. It is necessary to check the position of all fiducial markers before irradiation because fiducial markers may migrate or fall [22–25].

This study was performed with the assumption of SyncTraX imaging geometry. The markers could be identified in thicker PMMA phantoms through use of a higher-energy X-ray irradiation and short SID. However, the order of the image recognition performance will be maintained. Recently developed polymer and liquid markers may be difficult to use for RTRT, because their image contrast is lower than that of metal markers. Image-processing technique may be applied to detect such markers [26–28]. That will be addressed in future works.

In this study, template pattern matching was used for marker detection. The results may be varied according to the algorithm of marker detection, however comparison with other algorithm was not subject in this study. We have simulated one of the typical situations in the experiment. Actual clinical image will be varied for each treatment. For instance, the visibility of the marker in the liver could be decreased due to ribs and other bones in actual clinical situation.

## 5. Conclusion

This study was performed to quantitatively evaluate the image recognition performance of fiducial markers available for use in RTRT. Gold Marker, iGold, ACCULOC, ball-shaped Gold Anchor, and VISICOIL (0.75-mm and 1.0-mm diameter) were expected to be useful for liver and lung RTRT. Spherical markers and ACCULOC may be used for patients with more robust physical constitution. For two-dimensional images, image registration accuracy was < 2 pixels. Three-dimensional calculation error was thought to be < 1 mm for all fiducial markers. The results in this study may be useful for the selection of fiducial markers.

## Acknowledgement

The authors would like to thank Dr. Sugita, Dr. Uchida, and Ms. Ida for their helpful discussion and experimental support of this project.

## Funding

This research was partially supported by the Development of Medical Devices and Systems for Advanced Medical Services from Japan Agency for Medical Research and Development (AMED).

## References

- [1] Van der Horst A, Wognum S, Davila Fajardo R, de Jong R, van Hooft JE, Fockens P, et al. Interfractional position variation of pancreatic tumors quantified using intratumoral fiducial markers and daily cone beam computed tomography. *Int J Radiat Oncol Biol Phys* 2013;87:202–8.

- [2] Wunderink W, Mendez Romero A, Seppenwoolde Y, de Boer H, Levendag P, Heijmen B. Potentials and limitations of guiding liver stereotactic body radiation therapy set-up on liver-implanted fiducial markers. *Int J Radiat Oncol Biol Phys* 2010;77:1573–83.
- [3] Harada Keiichi, Katoh Norio, Suzuki Ryusuke, Ito Yoichi M, Shimizu Shinichi, Onimaru Rikiya, et al. Evaluation of the motion of lung tumors during stereotactic body radiation therapy (SBRT) with four-dimensional computed tomography (4DCT) using real-time tumor-tracking radiotherapy system (RTRT). *Phys Med* 2016;32:305–11.
- [4] Graf R, Wust P, Budach V, Boehmer D. Potentials of on-line repositioning based on implanted fiducial markers and electronic portal imaging in prostate cancer radiotherapy. *Radiat Oncol* 2009;4:13.
- [5] Handsfield LL, Yue NJ, Zhou J, Chen T, Goyal S. Determination of optimal fiducial marker across image-guided radiation therapy (IGRT) modalities: visibility and artifact analysis of gold, carbon, and polymer fiducial markers. *J Appl Clin Med Phys* 2012;13:181–9.
- [6] Gurney-Champion OJ, Lens E, van der Horst A, Houweling AC, Klaassen R, van Hooft JE, et al. Visibility and artifacts of gold fiducial markers used for image guided radiation therapy of pancreatic cancer on MRI. *Med Phys* 2015;42:2638–47.
- [7] Chen Y, O'Connell JJ, Ko CJ, Mayer RR, Belard A, McDonough JE. Fiducial markers in prostate for kV imaging: quantification of visibility and optimization of imaging conditions. *Phys Med Biol* 2012;57:155–72.
- [8] Chan MF, Cohen GN, Deasy JO. Qualitative evaluation of fiducial markers for radiotherapy imaging. *Technol Cancer Res Treat* 2015;14:298–304.
- [9] Schneider S, Jolck RI, Troost EGC, Hoffmann AL. Quantification of MRI visibility and artifacts at 3T of liquid fiducial marker in a pancreas tissue-mimicking phantom. *Med Phys* 2018;45:37–47.
- [10] Shirato H, Shimizu S, Kunieda T, Kitamura K, van Herk M, Kagei K, et al. Physical aspects of a real-time tumor-tracking system for gated radiotherapy. *Int J Radiat Oncol Biol Phys* 2000;48:1187–95.
- [11] Shimizu S, Miyamoto N, Matsuura T, Fujii Y, Umezawa M, Umegaki K, et al. A proton beam therapy system dedicated to spot-scanning increases accuracy with moving tumors by real-time imaging and gating and reduces equipment size. *PLoS One* 2014;9:e94971.
- [12] Regmi R, Lovelock DM, Hunt M, Zhang P, Pham H, Xiong J, et al. Automatic tracking of arbitrarily shaped implanted markers in kilovoltage projection images: a feasibility study. *Med Phys* 2014;41. 071906-1-11.
- [13] Gehrke C, Oates R, Ramachandran P, Deloar HM, Gill S, Kron T. Automatic tracking of gold seed markers from CBCT image projections in lung and prostate radiotherapy. *Phys Med* 2015;31:185–91.
- [14] Miyamoto N, Ishikawa M, Bengua G, Sutherland K, Suzuki R, Kimura S, et al. Optimization of fluoroscopy parameters using pattern matching prediction in the real-time tumor-tracking radiotherapy system. *Phys Med Biol* 2011;56:4803–13.
- [15] Block Alec M, Luce Jason, Lin Jeffrey Y, Hoggarth Mark A, Roeske John C. Planar IGRT dose reduction: A practical approach. *Pract Radiat Oncol* 2015;5:e239–44.
- [16] Anderson JA, Wang J, Clarke GD. Choice of phantom material and test protocols to determine radiation exposure rates for fluoroscopy. *Radiographics* 2000;20:1033–42.
- [17] Habermehl D, Henkner K, Ecker S, Jakel O, Debus J, Combs SE. Evaluation of different fiducial markers for image-guided radiotherapy and particle therapy. *J Radiat Res* 2013;54:61–8.
- [18] Matsuura T, Maeda K, Sutherland K, Takayanagi T, Shimizu S, Takao S, et al. Biological effect of dose distortion by fiducial markers in spot-scanning proton therapy with a limited number of fields: a simulation study. *Med Phys* 2012;39:5584–91.
- [19] Vassiliev ON, Kudchadker RJ, Kuban DA, Frank SJ, Choi S, Nguyen Q, et al. Dosimetric impact of fiducial markers in patients undergoing photon beam radiation therapy. *Phys Med* 2012;28:240–4.
- [20] Kupelian PA, Forbes A, Willoughby TR, Wallace K, Manon RR, Meeks SL, et al. Implantation and stability of metallic fiducials within pulmonary lesions. *Int J Radiat Oncol Biol Phys* 2007;69:777–85.
- [21] Ohta K, Shimohira M, Iwata H, Hashizume T, Ogino H, Miyakawa A, et al. Percutaneous fiducial marker placement under CT fluoroscopic guidance for stereotactic body radiotherapy of the lung: an initial experience. *J Radiat Res* 2013;54:957–61.
- [22] Persson GF, Josipovic M, von der Recke P, Aznar MC, Juhler-Notttrup T, Munck af Rosenschold P, et al. Stability of percutaneously implanted markers for lung stereotactic radiotherapy. *J Appl Clin Med Phys* 2013;14:187–95.
- [23] Jackson P, Steinfort DP, Kron T, Siva S. Practical assessment of bronchoscopically inserted fiducial markers for image guidance in stereotactic lung radiotherapy. *J Thorac Oncol* 2016;11:1363–8.
- [24] Shakir SI, Udrescu C, Enachescu C, Rouviere O, Arion S, Caraivan I, et al. Transrectal implantation and stability of gold markers in prostate bed for salvage radiotherapy of macroscopic recurrences. *Phys Med* 2016;32:1422–7.
- [25] Imura M, Yamazaki K, Shirato H, Onimaru R, Fujino M, Shimizu S, et al. Insertion and fixation of fiducial markers for setup and tracking of lung tumors in radiotherapy. *Int J Radiat Oncol Biol Phys* 2005;63:1442–7.
- [26] Miyamoto N, Ishikawa M, Sutherland K, Suzuki R, Matsuura T, Toramatsu C, et al. A motion-compensated image filter for low-dose fluoroscopy in a real-time tumor-tracking radiotherapy system. *J Radiat Res* 2015;56:186–96.
- [27] Chan CL, Katsaggelos AK, Sahakian AV. Image sequence filtering in quantum-limited noise with applications to low-dose fluoroscopy. *IEEE Trans Med Imaging* 1993;12:610–21.
- [28] Wilson DL, Jabri KN, Aufrichtig R. Perception of temporally filtered x-ray fluoroscopy images. *IEEE Trans Med Imaging* 1999;18:22–31.